JOURNAL OF THERMOPHYSICS AND HEAT TRANSFER
Vol. 7, No. 1, Jan.–March 1993

Numerical Modeling of a Slurry Droplet Containing a Spherical Particle

Constantine M. Megaridis*
University of Illinois at Chicago, Chicago, Illinois 60680
and
William A. Sirignano†
University of California, Irvine, Irvine, California 92717

A numerical investigation of the fundamental processes governing the momentum, energy, and mass exchanges between the solid, liquid, and gas phases of a vaporizing slurry droplet is presented. The axisymmetric configuration consists of an isolated slurry droplet with a large spherical solid particle in its core that is suddenly injected in a gaseous high-temperature, laminar, convective environment. The model allows for independent motion of the solid particle along the axis of symmetry of the slurry droplet, and considers variable gas-phase thermophysical properties as well as variable liquid-phase viscosities and latent heat of vaporization. Additional features of the model include internal liquid circulation with transient droplet heating, droplet surface regression due to vaporization, and droplet deceleration with respect to the free flow due to drag. The numerical calculation employs an iterative solution procedure that has been successfully used previously for an isolated all-liquid droplet. We found that the relative motion of the solid particle and the liquid-carrier fluid is very significant during the early stages of the simulation. In that respect, the fluid mechanics dominate the heat and mass transport phenomena involved, thus strongly suggesting a high possibility of secondary atomization as a result of the penetration of the solid particle through the gas/liquid interface.

Nomenclature

A = $[(a/a_p)^3 - 1]^{-1}$, coefficient used in Eq. (8)
a = a'/a'_0, instantaneous liquid droplet radius
a_p = a'_p/a'_0, solid particle radius
c'_p = specific heat of solid
c_{p_g} = c'_{p_g}/c'_{p_∞}, specific heat of gas at constant pressure
c_{pl} = specific heat of liquid
D_g = D'_g/D'_∞, gas-phase mass diffusion coefficient
Le_g = $\kappa'_\infty/(\rho'_\infty D'_\infty c'_{p_\infty})$, gas-phase Lewis number
Nu = Nusselt number
n = n'/a'_0, radial spherical coordinate
Pr_g = $\mu'_\infty c'_{p_\infty}/\kappa'_\infty$, gas-phase Prandtl number
Pr_l = $\mu'_{l,0} c'_{pl}/\kappa'_l$, initial liquid-phase Prandtl number
p = $(p' - p'_\infty)/(\rho'_\infty U'^2_{\infty,0})$, gas pressure
p_l = $(p'_l - p'_{l,\mathrm{ref}})/(\rho'_l U'^2_{\infty,0})$, liquid pressure
Re_g = $2a'_0 U'_{\infty,0}\rho'_\infty/\mu'_\infty$, initial gas-phase Reynolds number
Re_l = $2a'_0 U'_{\infty,0}\rho'_l/\mu'_{l,0}$, initial liquid-phase Reynolds number
r = r'/a'_0, radial cylindrical coordinate
Sh = Sherwood number
T = T'/T'_∞, temperature
t' = time
U_∞ = $U'_\infty/U'_{\infty,0}$, instantaneous freestream velocity
V = $V'/U'_{\infty,0}$, velocity component
V_d = $V'_d/U'_{\infty,0}$, velocity of droplet center with respect to a stationary frame
V_p = $V'_p/U'_{\infty,0}$, velocity of solid particle with respect to a stationary frame
Y_f = mass fraction of vaporizing fuel
z = z'/a'_0, axial cylindrical coordinate
γ = $\gamma' a'^2_0 \rho'_\infty/(U'_{\infty,0}\mu'_\infty)$, acceleration with respect to a stationary frame
ε = solid particle eccentricity with respect to geometric center of slurry droplet
θ = angular coordinate with respect to solid particle center
κ_g = κ'_g/κ'_∞, gas thermal conductivity
κ'_l = liquid thermal conductivity
κ'_p = solid thermal conductivity
μ = viscosity: μ'_g/μ'_∞, gas; $\mu'_l/\mu'_{l,0}$, liquid
ξ, η = generalized nonorthogonal coordinates
ρ_g = ρ'_g/ρ'_∞, gas density
ρ'_l = liquid density
ρ'_p = solid density
τ_{Es} = $t'\kappa'_p/(a'^2_0\rho'_p c'_p)$, nondimensional time normalized by thermal diffusion time in solid phase
τ_{Hg} = $t'\mu'_\infty/(a'^2_0\rho'_\infty)$, nondimensional time normalized by hydrodynamic diffusion time in gas phase
ϕ = angular coordinate with respect to geometric center of slurry droplet ($\phi = 0$; front stagnation point)
χ = $1 - T/T_c$, reduced temperature
ψ = $\psi'/(\rho'_l a'^2_0 U'_{\infty,0})$, stream function
ω = $\omega' a'_0/U'_{\infty,0}$, vorticity

Subscripts
av = spatial average
c = critical point
cm = c.m. of slurry droplet
f = liquid-carrier fuel
g = gas phase
gc = geometric center of slurry droplet
l = liquid phase
m = solid particle surface
n = normal direction
p = solid particle
r = radial direction in cylindrical coordinates
ref = reference value (arbitrary)
s = droplet surface
v = vapor
z = axial direction in cylindrical coordinates
0 = initial conditions
θ = tangential direction on solid particle surface

Received June 12, 1991; revision received March 27, 1992; accepted for publication March 30, 1992.

*Assistant Professor, Department of Mechanical Engineering. Member AIAA.
†Professor, Department of Mechanical and Aerospace Engineering. Fellow AIAA.

ϕ = tangential direction on liquid droplet surface
∞ = freestream conditions

Superscript
$'$ = dimensional quantity

Introduction

SLURRIES, defined as advanced multiphase fuels combining solid particles in liquid fuels, have attracted significant attention among the combustion community largely due to their wide employment in aerospace propulsion. The growing interest in fundamental research of slurry fuels is justified by the fact that solid particles, within high-temperature oxidative environments, burn and release substantial amounts of energy, thus showing important advantages over conventional all-liquid fuels. The liquid components of slurries serve both as a carrier and a fuel; therefore, slurry fuels have the advantage of the liquid-fuel properties (spray injectibility and pumpability) that make their utilization in aerospace applications very attractive. Even though slurry fuels are widely employed today, their vaporization, ignition, and combustion characteristics are not fully understood. A comprehensive review of the vaporization and combustion characteristics of slurry fuel droplets has been reported recently.[1]

A variety of solid constituents, such as aluminum, beryllium, boron, magnesium, and carbon have been studied so far with respect to their relative performance and degree of implementation to practical combustion systems. The majority of relevant investigations has been devoted to the latter stages of a slurry droplet lifetime, i.e., ignition and combustion.[2-4] However, only a few studies have examined the early stages of slurry droplet vaporization and the motion of the solid particles within the carrier liquid fuel. Chung[5] recently reported on the motion of small particles inside a liquid droplet. In the above study the influence of vaporization as well as the heat and mass transfer through the droplet surface were not taken into account. It was found that at high Reynolds numbers (Re) the solid particles tend to accumulate near the drop surface, while at low Re the particles remain evenly distributed throughout the bulk of the liquid droplet. The theoretical treatment of slurry droplets containing a single solid particle is far less advanced, since the interaction of solid and liquid phase complicates the analysis significantly. Petela[6] used a simplified model for the single-particle slurry droplet ignoring the liquid circulation, and assuming equal thermal diffusivities for both solid and liquid phases. The solid particle was assumed to maintain its concentric position with respect to the center of the droplet.

Sitarski[7] used a two-dimensional model to examine the vaporization dynamics of coal water slurry droplets suspended in their superheated vapor and irradiated from one side by a high-temperature blackbody radiation. The feasibility of secondary atomization was examined in that study and it was reported that microexplosion (explosive boiling) of irradiated droplets is more feasible at lower ambient gas temperatures and pressures.

Bhatia and Sirignano[8] developed a simplified spray model to examine the vaporization, ignition, and combustion characteristics of slurry droplets containing a large solid particle in their core. An axisymmetric and a spherically symmetric formulation were developed that gave very similar predictions for the cases considered. The solid particle core was assumed to maintain its concentric position with respect to the geometric center of the droplet throughout the simulations.

The current work focuses on understanding the details of the early postatomization stage of slurry droplet combustion, i.e., the dynamic interaction between solid and liquid phases, as well as the vaporization of the liquid carrier fuel. The details of the early stages of a slurry droplet lifetime are unraveled through quantitative, time varying, spatially resolved data in all three phases involved. An improved knowledge of the related processes would provide some important information on the practical implications involved.

Physical Description

The current study investigates the fluid mechanics along with the heating and vaporizing behavior of an isolated liquid droplet that contains a spherical particle in its core and is suddenly injected in a high-temperature, laminar, convective environment. This idealized configuration (depicted in Fig. 1) may be viewed as an approximation to a slurry droplet which contains a large solid particle or a small amount of liquid-carrier fluid. The flow considered is laminar and axisymmetric with initially uniform ambient conditions specified by $U'_{\infty,0}$, T'_∞, p'_∞, and $Y_{f,\infty} = 0$ (no fuel vapor in the incoming freestream). The solid particle, which is concentric with the surrounding liquid at the beginning of the simulation, is free to move along the axis of symmetry as a result of its dynamic interaction with the liquid carrier.

Soon after a slurry droplet with uniform temperature and no internal liquid motion is injected into the hot gas stream, a thin boundary layer is developed near the gas/liquid interface and a recirculation zone appears in the droplet gaseous wake.[9] The shear stress at the gas/liquid interface causes the gradual development of internal circulation within the liquid phase. The liquid is accelerated by the gas flow, and as it flows over the solid, exerts an axial force on the particle. The resulting relative motion of the solid particle and the carrier fluid has a very significant effect on the liquid-phase flow pattern. As the gas flow gradually adjusts to the presence of the droplet, the induced drag force effectively reduces the relative velocity between the droplet and the free flow, while the droplet size is simultaneously reduced due to vaporization. These combined events cause a gradual reduction of the droplet Reynolds number with time. The details of the solid particle motion with respect to the liquid-carrier fluid eventually determine the possibility for secondary atomization of the slurry droplet resulting from penetration of the particle through the liquid/gas interface. Such an event can be very desirable since it effectively reduces the time required for complete vaporization and combustion of the slurry droplet components.

Since the above momentum, heat, and mass transfer processes occur simultaneously, special care must be taken for their adequate representation in a detailed model configuration. Our model accounts for axial motion of the solid particle, variable thermophysical properties in the gas phase, variable viscosities and latent heat in the liquid phase, internal liquid circulation with transient droplet heating, droplet surface regression due to vaporization, and droplet deceleration with respect to the free flow. The current work extends the model of Chiang et al.[9] which was developed for an isolated, single-component, all-liquid droplet vaporizing inside a high-temperature convective environment. However, in the case of a slurry droplet, such as the one studied herein, the dynamic interaction of the solid particle and the liquid-carrier fluid introduces an additional degree of complexity on which the current study is mainly focused.

Assumptions and Governing Equations

The problem is physically viewed as an impulsively started, high-temperature flow over a fixed slurry droplet containing

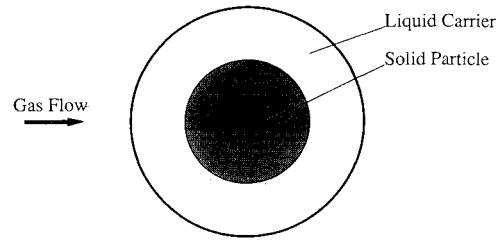

Fig. 1 Schematic of slurry-droplet flow configuration.

a concentric solid particle. Both liquid and solid components are initially at uniform temperatures. Instead of describing the droplet motion through the gas using an Eulerian formulation, we change the reference frame from a stationary laboratory coordinate system to a system moving with the geometric center of the droplet. As a result of the induced drag force, the relative velocity between the freestream and the droplet varies with time. In order to account for this change, an adjustment of the surrounding gas flowfield is necessary throughout the calculation. In addition, the drag force on the solid particle induced by the liquid phase motion around it, necessitates the monitoring of the particle location with respect to the geometric center of the slurry droplet throughout the calculation.

Since the flow studied herein is characterized by a low Mach number, the viscous dissipation terms have been neglected. The contributions of pressure and thermal gradients in gas-phase species diffusion have also been neglected. The very low pressure gradients associated with open systems, as the one under investigation, as well as the low values of the ratio of thermal diffusion coefficients to the product $\rho_g D_g$ for most gaseous mixtures justify our assumption. Gravity effects and radiative heat flux have also been neglected. The droplet deformation was not modeled since the droplets considered herein are characterized by low Weber numbers. In addition, the effects of surface tension have been neglected in the current formulation. The behavior of the gaseous mixture surrounding the droplet was assumed to be ideal, while all thermophysical properties (except viscosities and latent heat) in the liquid phase were considered invariant.

In the following we describe the additional considerations and adjustments to the all-liquid droplet model of Chiang et al.[9] that are needed to describe the slurry droplet and the motion of the solid particle. The nondimensional formulation introduced in Ref. 9 has been maintained in the current study. The initial droplet radius, freestream velocity and physical properties were used to nondimensionalize the variables. A cylindrical coordinate system (r, z) was employed to describe the axisymmetric geometry of the problem under investigation.

The detailed form of the applicable gas and liquid-phase equations, along with the appropriate boundary and initial conditions has been reported elsewhere[9] and will not be repeated here. The continuity, momentum, energy, and species equations were solved in the gas phase. The liquid phase surrounding the solid particle was described through a vorticity-stream function formulation[10,11] along with the energy equation. The addition of the solid-phase energy equation was necessary in order to account for the presence of the solid particle core within a slurry droplet:

$$\frac{\partial}{\partial \tau_{FS}}(rT) = \frac{\partial}{\partial r}\left(r\frac{\partial T}{\partial r}\right) + \frac{\partial}{\partial z}\left(r\frac{\partial T}{\partial z}\right) \tag{1}$$

Gas/Liquid and Solid/Liquid Interface Conditions

The overall behavior of the slurry droplet is highly sensitive to the gas/liquid interface conditions. The vapor pressure above the liquid surface was calculated using Wagner's equation[12] in the form

$$\ln\left(\frac{p_v'}{p_c'}\right) = \frac{\alpha_1\chi + \alpha_2\chi^{1.5} + \alpha_3\chi^3 + \alpha_4\chi^6}{1-\chi} \tag{2}$$

where $\chi = 1 - T/T_c$, and α_i; $i = 1, 4$ are coefficients[12] characteristic of the liquid compound. For n-octane, $\alpha_1 = -7.912$, $\alpha_2 = 1.380$, $\alpha_3 = -3.804$, and $\alpha_4 = -4.501$. The above equation has been shown[12] to give very good estimates of actual vapor pressure values determined in a wide range of experimental investigations and was chosen instead of the most commonly employed but less accurate Clapeyron equation for phase equilibrium. In addition, the principles of continuity for shear stress, tangential velocity, mass flux, temperature, energy, and species fluxes were expressed in terms of the relevant variables as a system of equations[9] solved sequentially within the overall iterative solution procedure. This system relates the events occurring in the gas phase to those within the droplet.

The continuity of temperature and heat flux on the solid/liquid interface was expressed in spherical coordinates (n, θ) as

$$T_p|_m = T_l|_m, \qquad \kappa_p' \left.\frac{\partial T_p}{\partial n}\right|_m = \kappa_l' \left.\frac{\partial T_l}{\partial n}\right|_m \tag{3}$$

The liquid-phase vorticity over the solid-particle surface, also expressed in spherical coordinates, is given by

$$\omega = -\frac{\partial V_{l,\theta}}{\partial n} - \frac{V_{l,\theta}}{a_p} + \frac{1}{a_p}\frac{\partial V_{l,n}}{\partial \theta} \tag{4}$$

Finally, the liquid-phase stream function over the solid-particle surface is given by

$$\psi = \frac{r^2}{2}(V_d - V_p) \tag{5}$$

where the axial velocities of the geometric center of the droplet V_d and the solid particle V_p are expressed with respect to a stationary frame. It is important to note that the substantial relative motion of the solid particle and the geometric center of the slurry droplet results in nonzero values of the stream function of the particle surface. This is apparent from the boundary condition for the stream function as defined by Eq. (5).

Solid Particle Drag

The determination of the drag force which is exerted on the solid particle as a result of the liquid motion requires knowledge of the velocity and pressure distributions within the liquid phase directly above the particle surface. The required velocities are readily calculated from the liquid-phase stream function values. However, since the pressure in the liquid phase is not calculated directly, we need to solve the tangential component of the liquid momentum equation on the particle surface. This equation, expressed in spherical coordinates with respect to a reference frame based on the center of the solid particle and moving with the velocity of the center of the droplet, is given by

$$\frac{\partial p_l}{\partial \theta} = \frac{2\mu_l}{Re_l}\left(a_p\frac{\partial^2 V_\theta}{\partial n^2} + \frac{1}{3}\frac{\partial^2 V_n}{\partial n \partial \theta} + 2\frac{\partial V_\theta}{\partial n} - \frac{2}{3}\cot\theta\frac{\partial V_n}{\partial n}\right) - \frac{2a_p\sin\theta}{Re_g}\gamma_p - a_p(V_n - V_d\cos\theta)\frac{\partial V_\theta}{\partial n} \tag{6}$$

Low spatial variations of the liquid viscosity were assumed in the derivation of Eq. (6). The first term of the right side of the above equation arises from the viscous terms of the momentum equation, while the second term describes an external body force due to the solid particle acceleration at a rate γ_p. The third term on the right side of Eq. (6) arises from the convective terms of the momentum equation and includes the velocity of the geometric center of the droplet V_d as a result of a change in the reference frame.

Equation (6) gives the pressure distribution on the solid particle surface by a simple integration along θ, when the pressure at $\theta = 0$ is used as a reference value. The acceleration of the solid particle with respect to a stationary frame, which results from the induced drag force, may then be expressed as a sum of the pressure and friction contributions given by

$$\gamma_p = \frac{3Re_g}{4a_p^3}\frac{\rho_l'}{\rho_p'}\int_0^\pi p_l(\varepsilon - z)r\,d\theta + \frac{3}{2a_p^3}\frac{\mu_{l,0}'}{\mu_z'}\frac{\rho_z'}{\rho_p'}\int_0^\pi\left[r\frac{\partial V_\theta}{\partial n} + \frac{4}{3}(z-\varepsilon)\frac{\partial V_n}{\partial n}\right]\mu_l r\,d\theta \tag{7}$$

where ε is the eccentricity of the solid particle center with respect to the geometric center of the slurry droplet.

As seen from the above, the pressure above the solid-particle surface and the solid-particle acceleration are related in an intricate integro-differential manner expressed by Eqs. (6) and (7). These two equations describe the dynamic interaction of the liquid and the solid phase. Numerical integration of Eq. (6) is performed to determine the pressure distribution $p_l(\theta)$ assuming a known value of γ_p. An updated value for γ_p is subsequently obtained from Eq. (7) using the pressure distribution $p_l(\theta)$ calculated from Eq. (6).

Treatment of Solid-Particle Motion

As mentioned previously, the liquid-phase motion over the solid particle results in a drag force exerted on the particle along the axis of symmetry. As a result of the generally unequal liquid and solid accelerations, a separation of the particle center from the geometric center of the slurry droplet occurs. The geometric center of the slurry droplet also coincides with the origin of the liquid-phase-motion reference frame. The above separation is expressed as the distance between the center of the solid particle from the geometric center of the slurry droplet and is denoted as eccentricity ε. The displacement of the particle causes the eccentric positioning of the c.m. of the slurry droplet as well. The relative axial motion of all three points of interest, i.e., center of solid particle, c.m., and geometric center of the slurry droplet, is monitored throughout the calculation. The acceleration of the geometric center of the droplet is related to the acceleration of its c.m. and the acceleration of the solid particle through the following equation:

$$\gamma_{gc} = \frac{1 + A\rho_p'/\rho_l'}{1 + A}\gamma_{cm} + \frac{A}{1 + A}\left(1 - \frac{\rho_p'}{\rho_l'}\right)\gamma_p \qquad (8)$$

where $A = [(a/a_p)^3 - 1]^{-1}$. The above equation does not consider the effect of the liquid surface regression due to vaporization.

The acceleration of the c.m. of the slurry droplet γ_{cm} is calculated at each instant through the drag force exerted on the droplet as a result of the gas flow around it. The details of the drag force calculation are reported elsewhere.[9] As mentioned in the previous section, the acceleration of the solid particle γ_p is calculated from the drag force exerted on the particle as a result of the liquid flow around it. The velocities of the three points of interest are updated throughout the simulation using the calculated values of the respective accelerations. The knowledge of the velocities and accelerations of the solid particle and the geometric center of the slurry droplet results in the timewise determination of the eccentricity of the solid particle with respect to the origin of the reference frame, and therefore, of the relative position of solid and liquid throughout the simulation.

Numerical Solution Procedure

Before attempting a numerical solution, the related equations were transformed to generalized nonorthogonal coordinates (ξ, η), which allow for any arbitrary shaped body as well as for changes in droplet radius with time due to vaporization. The nonlinear, highly coupled equations describing the slurry droplet dynamics were discretized by implicit finite-difference schemes. The conditions employed for the boundaries of the computational domain were identical to those used in Ref. 9, with the exception of the outflow condition for pressure that was substituted by the condition $\partial_p/\partial_z = 0$. The calculations were performed on a rectangular mesh with equal spacings ($\Delta\xi = \Delta\eta = 1$). The iterative solution procedure requires the calculation of the Jacobian and other metrics of the transformation anytime the grid is adjusted to conform to the motion of the solid particle along the axis and the regressing droplet surface.

The model allows for independent motion of the solid particle within the bulk of the surrounding liquid. The forces exerted by the liquid-flow motion (pressure field and viscous stress contributions) on the solid particle along its axis of symmetry are used sequentially to adjust the position of the solid particle core with respect to the geometric center of the slurry droplet. This feature allows the monitoring of the relative motion of the two components (solid, liquid) of the slurry droplet and provides important data on a problem that has not been addressed yet in relevant investigations. Our simulations showed that the rapid motion of the solid particle with respect to the liquid phase eventually resulted in grid Peclet numbers appreciably higher than unity. For this reason, a hybrid (central difference/upwind) discretization scheme was employed for the convective terms of both energy and vorticity equations in the liquid phase.[13]

The developed numerical code employs an iterative solution procedure[9] for the determination of the fields of interest in the solid, liquid, and gas phases, and calculates the related drag coefficients and transfer numbers.[9] Two checks were performed on the reliability of the results obtained using the numerical model. The first involved the influence of the computational far-field distance from the center of the slurry droplet. We found that a distance $r_\infty = 16\alpha_0$ was adequate in order to obtain far-field independent results. The second check examined the grid and time-step dependence of the results. We found that a grid of 71 × 41 nodes and a time step of $\Delta\tau_{Hg} = 8 \times 10^{-4}$ were needed in order to assure grid and time-step independence. The fine grid in concert with the great disparity of the characteristic time scales involved (thus necessitating a fine time step), required extensive computations that were performed on a CRAY Y-MP and a CONVEX-240 supercomputer.

Results and Discussion

The base case calculation was selected to simulate a liquid *n*-octane droplet of initial radius a_0' containing a concentric aluminum particle of radius $a_0'/2$. The slurry droplet is assumed to be initially at a uniform temperature $T_0' = 300$ K. This droplet is suddenly ($t' = 0$) injected in a uniform airstream characterized by a velocity $U_{\infty,0}'$, a temperature $T_\infty' = 1250$ K and a pressure $p_\infty' = 10$ atm. The initial Reynolds number was selected to be $Re_g = 2U_{\infty,0}'a_0'\rho_\infty'/\mu_\infty' = 50$ at the beginning of the simulation. The values of physical parameters and nondimensional groups employed in the base case calculation are given in Table 1. These conditions correspond to an initial solid mass fraction of 36% that is on the low end of the range observed in realistic slurry droplet applications.

The computational mesh employed in the gas phase consisted of 37 (radial direction) × 41 (angular direction) nodes, while a mesh of 24 (radial direction) × 41 (angular direction) was employed for the liquid phase. The liquid-phase grid concentration was higher above the solid surface and below the gas/liquid interface. A mesh of 10 × 41 was used for the solid phase. As mentioned previously, the grid locations have to be adjusted continuously in order to accommodate the motion of the solid particle with respect to the geometric center of the slurry droplet, as well as the droplet surface regression due to vaporization. The base case calculation was carried only to nondimensional time $\tau_{Hg} = 1.5$ due to the rise of strong oscillations of the velocity and pressure fields over the solid-particle surface. A discussion relevant to this behavior follows after the presentation of the results during the stable period. At the instant of termination of the simulation only 0.6% of the available liquid mass had vaporized.

The gas-phase contours for the slurry droplet calculation resemble those calculated in the case of an all-liquid droplet.[9] However, the liquid-phase contours are significantly affected by the presence and motion of the solid particle. Figure 2 displays the liquid-phase streamlines (upper half) and velocity vectors (lower half) at an instant $\tau_{Hg} = 1$ of the base case simulation. The velocities were calculated from the stream

Table 1 Physical parameters used in base case slurry droplet simulation

Parameter	Value
Initial Reynolds number, gas phase $Re_g = 2a'_0U'_\infty\rho'_\infty/\mu'_\infty$	50
Solid particle radius	$a'_0/2$
Freestream temperature, K	1250
Ambient pressure, atm	10
Initial slurry droplet temperature, K	300
Prandtl number Pr_g, gas phase	0.74
Initial Prandtl number Pr_l, liquid phase	9.38
Lewis number Le_g, gas phase	3.20
Molecular weight, air, kg/kmol	28.96
Molecular weight, *n*-octane, kg/kmol	114.2
Latent heat at normal boiling point (398.8 K), *n*-octane, kJ/kg	303.3
Liquid/gas viscosity ratio at time = 0, $\mu'_{l,0}/\mu'_\infty$	11.44
Liquid/gas conductivity ratio, κ'_l/κ'_∞	1.69
Solid/liquid conductivity ratio, κ'_p/κ'_l	1581
Liquid/gas density ratio, ρ'_l/ρ'_∞	252
Solid/liquid density ratio, ρ'_p/ρ'_l	3.87
Liquid/gas specific heat ratio at constant pressure, $c'_{pl}/c'_{p\infty}$	1.87
Solid/liquid specific heat ratio, c'_p/c'_{pl}	0.4

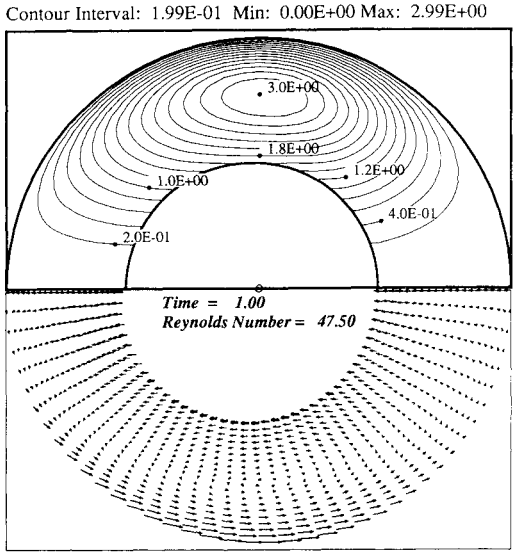

Fig. 2 Liquid-phase streamlines (upper half) and velocity vectors (lower half) at $\tau_{Hg} = 1$ of the base case slurry simulation. The outer circle represents the gas/liquid interface, while the inner one represents the solid-particle surface. The ambient gas flow is directed from left to right.

function values and have been expressed with respect to a reference frame moving with the geometric center of the droplet which is indicated by a circle on the axis of symmetry. The development of a vortex directly above the solid-particle surface is apparent in this figure. The vortex, which is asymmetric with respect to the vertical axis through the center of the slurry droplet, moves clockwise towards the aft of the droplet during the simulation. It is worth noting that the solid-particle surface is not a streamline due to the significant relative motion of the solid with respect to the geometric center of the slurry droplet. This relative motion is clearly demonstrated by the liquid-phase velocity vector field at the same instant. A sequence of figures similar to Fig. 2 showed that the liquid/gas interface velocities and the relative velocity of the solid particle with respect to the center of the droplet increase monotonically with time. As also seen on Fig. 2, the maximum liquid velocities occur on the liquid/gas interface and near the vortex region. The axial motion of the solid particle within the liquid volume enhances the liquid circulation which is initiated on the droplet surface due to shear interaction of the liquid droplet and the gas flow. The increasing relative velocity between the solid and the liquid results in increasingly higher eccentricities ε.

Figure 3 shows the spatial variations of the isothermal contours in the slurry droplet interior at three different times of the base case simulation ($\tau_{Hg} = 0.5$, 1, and 1.5). During the very early stages of the simulation (Fig. 3a), a thermal boundary layer is rapidly formed within the liquid regions adjacent to the droplet surface. The steep temperature gradients associated with this layer result in conductive transfer of energy from the gas/liquid interface to the inner regions of the droplet. Simultaneously, the convective mechanisms, which develop as a result of the exposure of the droplet surface to the gas flow, transfer hot liquid from the gas/liquid interface to the droplet interior. This convective transfer results in the exposure of the solid material to heated liquid which is transported over its surface (Fig. 3b). Due to the high conductivity of the metal considered herein (aluminum), the temperature within the particle remains spatially uniform even though it is temporally varying. The form of the temperature contours at later times (Fig. 3c) suggest the importance of the convective mechanisms in the transfer of energy within the liquid phase at this stage of the calculation. As it will be shown in the following, the thermal pattern indicated in Fig. 3 is reinforced by the significant relative motion of the solid with respect to the liquid-carrier fluid.

The relative motion of the solid particle with respect to the c.m. and the geometric center of the slurry droplet is monitored by the time variations of the corresponding velocities. Figure 4 shows the time variation of the axial velocities of the three centers of interest with respect to a stationary frame for the base case calculation; namely, the center of the solid particle, the c.m. and the geometric center of the slurry droplet. It is apparent that the geometric center of the droplet moves faster than its center of mass, while the solid particle remains essentially stationary throughout the simulation, thus indicating a monotonically increasing eccentricity ε.

A series of figures, showing the angular variation of several quantities on the solid/liquid and the liquid/gas interface, is used to assess the flowfield within and around the slurry droplet as well as the importance of the convective effects. The time variation of the angular distribution of the solid-particle surface temperature was initially investigated. The high conductivities of the solid phase resulted in almost spatially uniform surface temperatures throughout the simulation. Our observations consistently showed that the aluminum phase remains essentially isothermal, even though its temperature is temporally varying during the calculations.

The angular variation of pressure over the solid-particle surface is depicted in Fig. 5 at three different instants of the base case calculation ($\tau_{Hg} = 0.4$, 0.8, and 1). The pressure at $\theta = 0$ deg is used as a reference value. As seen in Fig. 5, the pressures above the particle surface are consistently higher than the reference pressure, except at regions with 160 deg

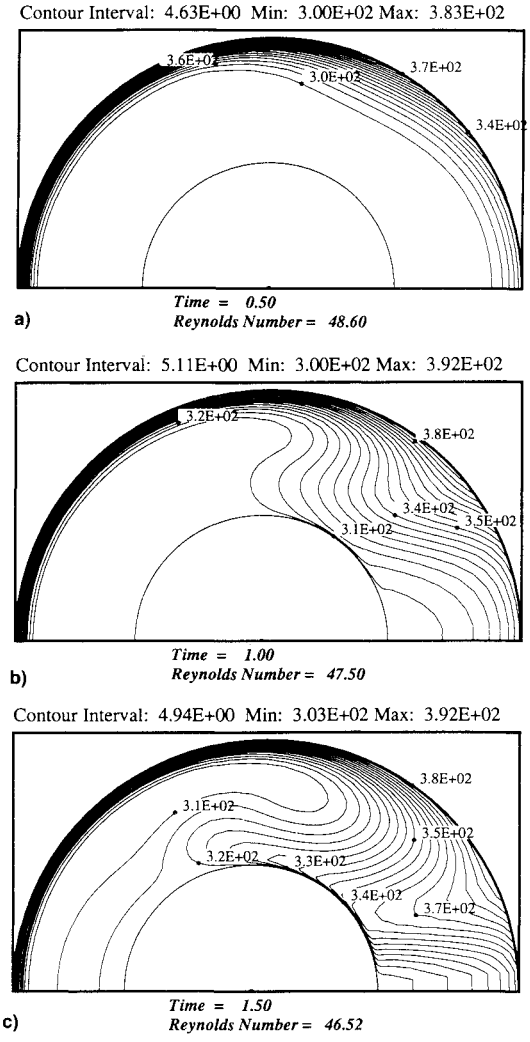

Fig. 3 Liquid-phase isothermal contours at three different times of the base case slurry simulation: a) τ_{Hg} = 0.5, b) τ_{Hg} = 1, and c) τ_{Hg} = 1.5. The outer circle represents the gas/liquid interface, while the inner one represents the solid particle surface. The gas flow is directed from left to right.

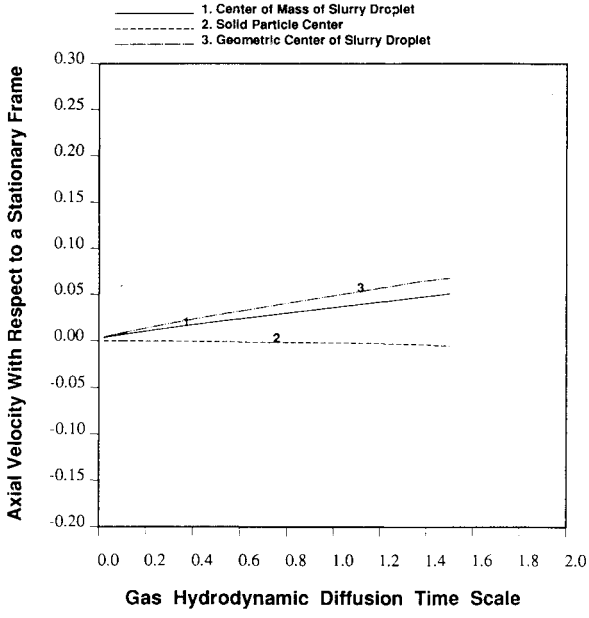

Fig. 4 Time variation of the velocities of the three centers of interest in the base case slurry droplet simulation. These velocities are expressed with respect to a stationary reference frame.

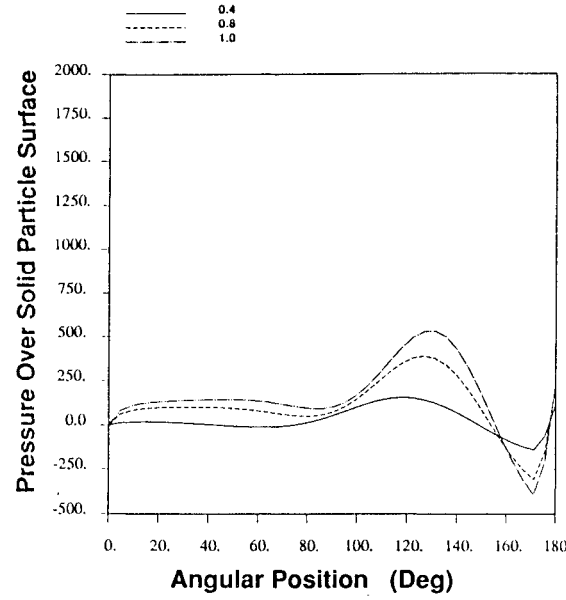

Fig. 5 Angular variation of pressure differential (in N/m²) over the solid-particle at three different times of the base case simulation (τ_{Hg} = 0.4, 0.8, and 1). The pressure at θ = 0 deg over the solid surface was used as a reference value.

$< \theta <$ 180 deg. The higher pressures around $\theta \approx$ 130 deg result in a force pushing the solid particle in the upstream direction with respect to the liquid flow. In essence, the angular variation of $p_l(\theta)$ at a specific instant (as depicted in Fig. 5) was obtained by a simple numerical integration of Eq. (6). The importance of the terms on the right side of Eq. (6) was investigated by examining their relative magnitude. We found that the term containing the particle acceleration γ_p was rather insignificant, especially when compared to the viscous term $\partial^2 V_\theta/\partial n^2$. The importance of these terms was investigated by neglecting their respective contributions in Eq. (6) and examining the effect on the liquid-phase fields and some global quantities (primarily the corresponding values of ε). Even though the angular distribution of pressure over the solid particle, as displayed in Fig. 5, could be interpreted as a strong pseudohydrostatic effect on the rear side of the particle ($\theta \approx$ 180 deg), our analysis showed that the particle acceleration term does not significantly contribute to the calculated values of $p_l(\theta)$. This unusual pressure result might be attributed to the nonuniformity of the liquid flow around the particle, combined with the bounded character of the liquid flowfield.

Figure 6 depicts the angular variation of the tangential velocity V_ϕ at four different times of the base case simulation (τ_{Hg} = 0.4, 0.8, 1, and 1.4). As seen, there is a strong tangential acceleration of the liquid surface throughout the simulation. The above values of V_ϕ are very similar to those obtained in the all-liquid droplet calculation by Chiang et al.[9] This suggests that the presence of the solid particle within the liquid bulk does not significantly alter the gas/liquid interface motion. It will be shown in the following, that even though this result is counter-intuitive, it can be attributed to the lagging motion of the solid particle with respect to the liquid surrounding it.

Figure 7 shows the angular variation of temperature on the gas/liquid interface at four different times of the base case simulation (τ_{Hg} = 0.4, 0.8, 1, and 1.4). The temperature of the liquid surface is clearly spatially nonuniform, with slightly higher values than those calculated by Chiang et al.[9] for the all-liquid droplet. At each instant, both points of maximum and minimum temperature for the slurry-droplet surface correspond to locations adjacent to the recirculating wake in the aft of the droplet. This is a result of the presence of the vortex within the liquid, which enhances the heat-transfer mechanisms in a substantial way. The base case simulation showed that, in contrast to the temperature angular distribution, the

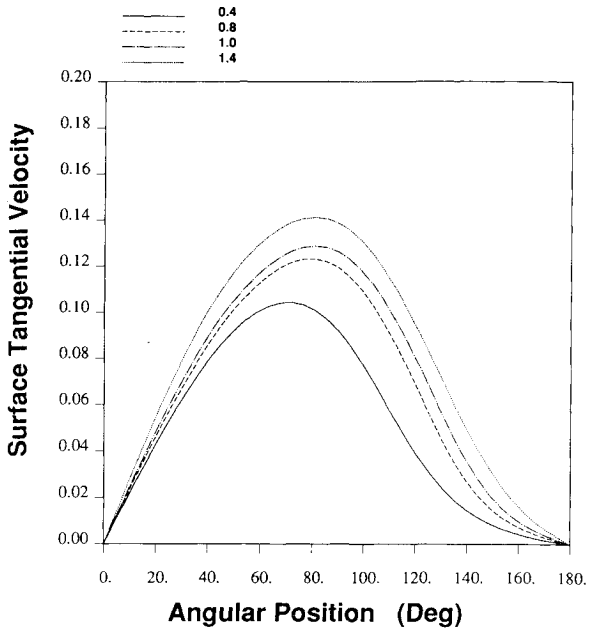

Fig. 6 Angular variation of tangential velocity on the gas/liquid interface at four different times of the base case simulation (τ_{Hg} = 0.4, 0.8, 1, and 1.4).

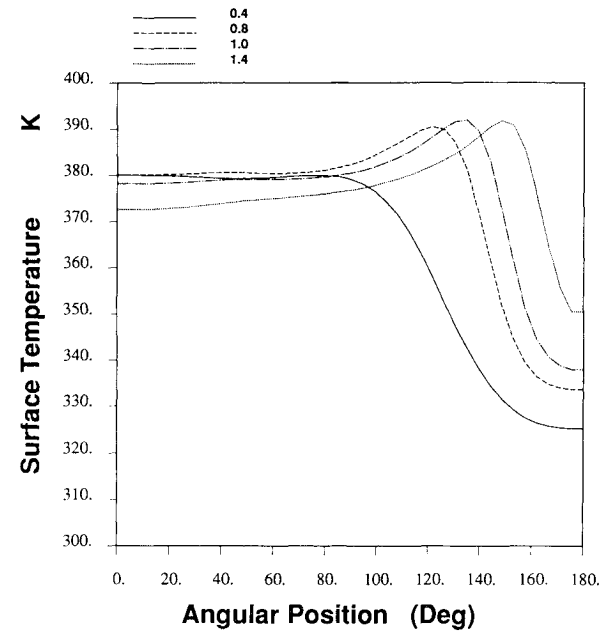

Fig. 7 Angular variation of temperature on the gas/liquid interface of the slurry droplet at four different times of the base case simulation (τ_{Hg} = 0.4, 0.8, 1, and 1.4).

maximum value of the local $Nu = 2a\kappa_g(\partial T_g/\partial n)/(1 - T)$ corresponds to the front stagnation point of the slurry droplet. In addition, the values of the local Nu remained almost unchanged throughout the simulation. The angular variation of the local $Sh = 2a\rho_g D_g(\partial Y_f/\partial n)/(Y_{f,\infty} - Y_f)$ on the gas/liquid interface also displayed maximum values at the front stagnation point of the flow. The temporal variation of Sh was very weak at all angles with the exception of the regions near the recirculating wake.

Figure 8 depicts the angular variation of the vaporization mass flux ($\rho_g V_{g,n}$) over the liquid surface at four different times of the base case simulation (τ_{Hg} = 0.4, 0.8, 1, and 1.4). Since the liquid-surface temperatures are relatively low, the associated vaporization fluxes are not substantial. This figure, however, clearly demonstrates the nonuniformity of the vaporization flux over the surface of a droplet in a convective environment. The flux peaks at regions close to the front

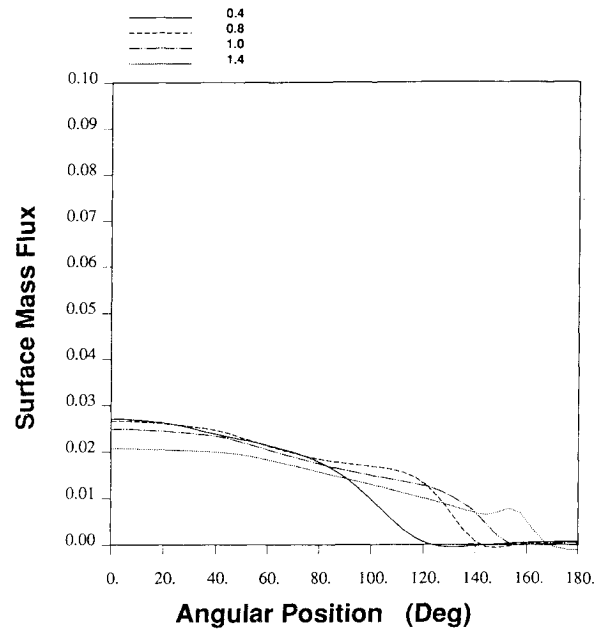

Fig. 8 Angular variation of vaporization mass flux ($\rho_g V_{g,n}$) on the gas/liquid interface at four different times of the base case simulation (τ_{Hg} = 0.4, 0.8, 1, and 1.4).

stagnation point of the slurry droplet. It should be also noted that, even though the maximum of the surface temperature occurs at regions closer to the recirculating wake (Fig. 7), the vaporization flux does not follow this behavior. This is primarily because the vaporization rate depends strongly on the local convective gas-phase conditions which are very intense near the front stagnation point of the flow ($\phi \approx 0$ deg). Some slightly negative values of the vaporization flux at the aft of the droplet (Fig. 8) suggest some condensation of the liquid vapor, mainly due to the relatively low local surface temperatures (Fig. 7) and the accumulation of fuel vapor in the recirculating wake region.

As mentioned previously, the base case calculation was terminated at τ_{Hg} = 1.5 when strong oscillations of the velocity and pressure fields over the solid-particle surface caused unstable temporal behavior of the particle accelerations. Further investigation of this behavior showed that the instability originates at $\tau_{Hg} \approx 1.3$ from the term $\partial^2 V_\theta/\partial n^2$ of Eq (6) thus rendering the results of the calculations unreliable after τ_{Hg} = 1.5. Prior to that time, the calculated quantities of the gas/liquid interface displayed normal behavior. The time of first appearance of the instability was not affected by changes in the solid-particle size and properties. Also, the solution behavior prior to the onset of instability was highly insensitive to the computational grid and the utilized time step. The origin of the instability was investigated by running two additional simulations with different Reynolds numbers (Re_g = 100, 20). These simulations revealed a dramatic change for the time of first appearance of the instability. The case with Re_g = 100 showed unstable behavior appearing after $\tau_{Hg} \approx 0.7$, while the Re_g = 20 case showed a delayed appearance ($\tau_{Hg} \approx 3.7$) of the pressure oscillations. By monitoring the temporal variation of the liquid-phase Reynolds number based on solid-particle diameter and relative velocity between solid and liquid, we found that for all cases at the time of initiation of the above instability the liquid-phase Reynolds number was of the order of 100.

Further investigation of the source of unstable behavior over the solid/liquid interface showed the time of first appearance of the instability to be very sensitive to the value of the relaxation factor ω employed in the numerical solution of the liquid-phase stream function equation.[9] Certain values of the relaxation factor ω (1.2, 1.5, and 1.8) were studied in the sensitivity analysis. We found that the value ω = 1.5 delayed

the onset of instability the most. For the other values of ω, unstable behavior was initiated over the particle surface at much earlier stages of the corresponding simulation. Experience[14] indicates that an optimal value of ω exists for maximizing the rate of convergence. Our observations strongly suggest that the unstable behavior experienced by the model is numerical. However, the high degree of consistency of the model predictions for $\omega = 1.5$ during the stable period supports the view that the model provides reliable data during that period.

The above numerical instability appears to be a result of the strong dynamic interaction of the liquid and solid phases. We should emphasize that our axisymmetric calculation would be inadequate to resolve three-dimensional effects. In addition, the assumption of sphericity for the slurry droplet may also be inadequate when the relative velocity between solid and liquid becomes very important. Even though our model cannot adequately represent the slurry droplet dynamic and thermal behavior at later stages, it does provide some important insight for the early stable period.

Figure 9 shows the absolute values of the solid-particle eccentricities (ε) with respect to the geometric center of the slurry droplets for the three different values of initial Reynolds number based on droplet diameter and relative velocity between gas and liquid at the time of injection. The actual values of ε are always negative due to the choice of the coordinate system. The termination of a curve indicates the end of the stable period. It is apparent from Fig. 9 that higher values of Re_g cause the solid particle to separate from the slurry droplet center at a faster rate, thus causing larger values of $|\varepsilon|$.

The effects of solid-particle size and density during the stable period were investigated with our slurry droplet model. In addition to the base case calculation ($a_p = 0.5$, $\rho_p' = 2{,}707$ kg/m^3, $\rho_l' = 700$ kg/m^3), two other cases were studied; one with a solid particle of radius $a_p = 0.5$ and density $\rho_p' = 1{,}760$ kg/m^3, and another with a solid particle of density $\rho_p' = 2{,}707$ kg/m^3 and radius $a_p = 0.397$, corresponding to a solid volume half of that used in the base case calculation. For both additional simulations, the liquid-phase density employed was $\rho_l' = 835$ kg/m^3 in order to maintain the mass of the slurry droplet identical to that used in the base case calculation. These two additional slurry droplet cases are denoted as "lower solid-density" and "half solid-volume" calculations, respectively. The corresponding solid mass fractions are 23 and 18%, respectively. All other parameters used in these calculations were identical to those employed in the base case simulation. Even though the two cases mentioned above describe slurry droplets with the same total mass, the corresponding solid-particle masses are not identical. More specifically, the "lower solid-density" particle is 35% lighter than the base case solid particle, while the half solid-volume particle is 50% lighter than the base case solid particle. The accelerations of the above slurry droplets with respect to a stationary frame maintained values much higher than the gravity value, therefore, our assumption of negligible gravity effects is justified a posteriori.

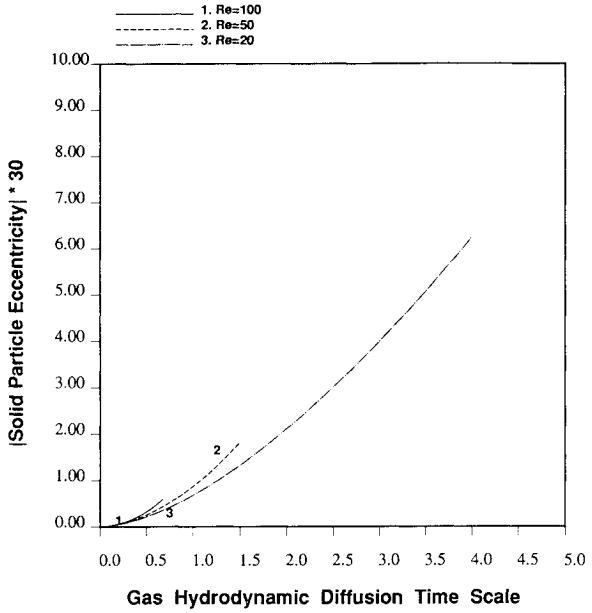

Fig. 9 Time variation of solid particle eccentricities for three slurry droplets with different initial Reynolds numbers (Re_g = 100, 50, and 20). The eccentricity is defined as the distance of the solid particle center from the geometric center of a slurry droplet.

Figure 10 shows the absolute values of the solid-particle eccentricities for the three slurry cases considered with $Re_g = 50$. For all three cases, the droplets are characterized by the same mass and are accelerated by identical gas streams. It is apparent from Fig. 10 that the heavier solid particle within the base case slurry droplet tends to separate from the droplet center faster than the lighter particles in the lower solid-density and half solid-volume calculations. The above behavior can be physically explained when we compare the forces acting on the solid particle. The drag force, which acts on the solid particle as a result of the liquid-phase motion around it, tends to decrease the values of $|\varepsilon|$ and is proportional to the square of the particle radius ($\propto a_p^2$). On the other hand, the solid-particle inertia tends to increase the values of $|\varepsilon|$ and is proportional to the product of the solid density and the cube of the particle radius ($\propto \rho_p a_p^3$). This reasoning leads to the conclusion that the displacement of the solid particle from the geometric center of the slurry droplet changes according to the product $\rho_p a_p$, therefore, the trends depicted in Fig. 10 are physically expected. As also shown by the same figure, the eccentricity of the solid particle along the axis of symmetry with respect to the geometric center of the slurry droplet becomes very substantial early in the lifetime of the droplet. This displacement is very significant, as clearly demonstrated by the liquid-phase fields displayed in Figs. 2 and 3. The increasingly faster rates of solid-particle separation from the geometric center of the slurry droplet strongly suggest a high possibility of secondary atomization at a subsequent stage. Such an event in a practical system would significantly enhance the liquid vaporization and would expose the solid particle to the hot environment of the combustion gases at an early stage.

Figure 11 compares the time variation of the average liquid-surface and solid temperatures for the three slurry droplets

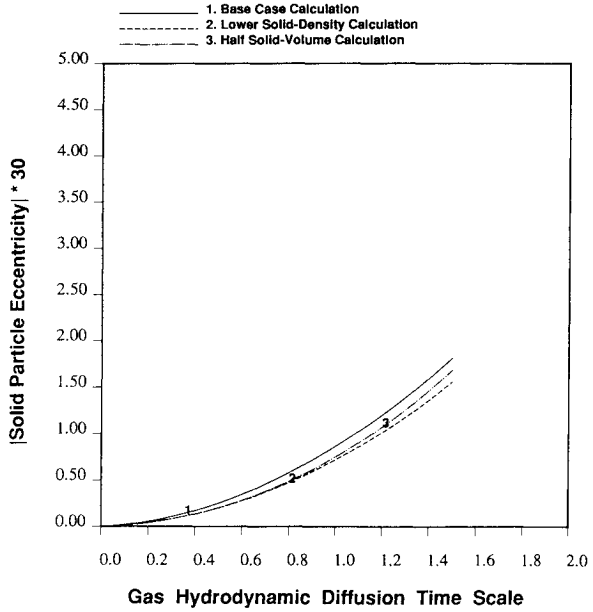

Fig. 10 Time variation of solid particle eccentricities $|\varepsilon|$ for the three slurry droplet cases studied.

considered herein. The liquid-phase temperatures show that the base case slurry droplet surface heats up faster compared to the other two. It is also apparent that there is a significant lapse between the time that the liquid phase starts heating up and the instant the solid phase starts absorbing a significant amount of heat depicted by a gradual temperature increase. Since the simulation was only carried to $\tau_{Hg} = 1.5$ the solid temperatures remained substantially lower than those on the liquid surface. Finally, the time variation of droplet drag coefficients showed almost identical values for all three cases compared herein.

The results obtained for the slurry simulations during the early stable period were compared to those obtained by Chiang et al.[9] for an all-liquid droplet. The relatively short periods of the slurry droplet lifetime resolved herein do not allow firm conclusions for later stages where the vaporization would be more vigorous.

The comparisons of slurry and all-liquid droplet results at the early stages of the droplet lifetime were performed using two gas/liquid interface quantities. First, the surface-averaged Nusselt number which is given by

$$Nu_{av,s} = \frac{a \int_0^{\pi} \kappa_g \frac{\partial T_g}{\partial n} \sin \phi \, d\phi}{1 - T_{av,s}} \tag{9}$$

with the surface-averaged temperature $T_{av,s}$ calculated from

$$T_{av,s} = \frac{1}{2} \int_0^{\pi} T \sin \phi \, d\phi$$

Second, the surface-averaged Sherwood number which is given by

$$Sh_{av,s} = \frac{a \int_0^{\pi} \rho_g D_g \frac{\partial Y_f}{\partial n} \sin \phi \, d\phi}{Y_{f,av,\infty} - Y_{f,av,s}} \tag{10}$$

where the average gas-phase mass fractions are calculated from

$$Y_{f,av} = \frac{1}{2} \int_0^{\pi} Y_f \sin \phi \, d\phi$$

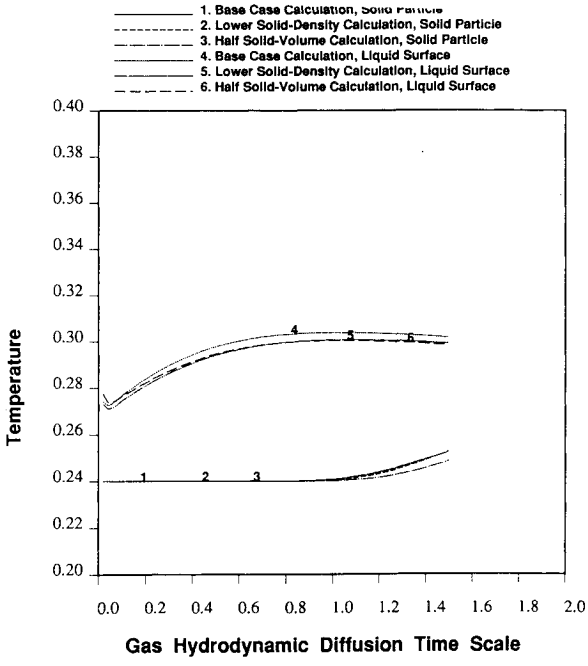

Fig. 11 Time variation of surface-averaged temperature on the gas/liquid interface and solid-particle temperature for the three slurry droplet cases studied.

The time variation of $Nu_{av,s}$ showed that the values of the heat transfer coefficient remain almost unchanged throughout all three slurry simulations except during the very early stages when $Nu_{av,s}$ shows a monotonically decreasing behavior. The corresponding values are nearly the same for all the slurry droplets, staying consistently above the all-liquid droplet values. The time variation of $Sh_{av,s}$ for the four cases studied showed very similar values at all times, except during the very early stages of the simulation. This suggests that the presence of a large solid particle inside a liquid droplet does not significantly affect the mass transfer coefficients across the gas/liquid interface. We should emphasize, though, that our comparisons of slurry and all-liquid droplets are applicable during the very early stages of a droplet lifetime. Subsequent trends may be substantially different.

Conclusions

A numerical investigation of the fundamental processes governing the momentum, energy, and mass exchanges between the solid, liquid, and gas phases of a slurry droplet suddenly injected in a hot-gas stream is presented. The axisymmetric configuration studied consists of an isolated slurry droplet containing a solid particle in its core and vaporizing in a laminar convective environment. The model allows for independent motion of the solid particle along the axis of symmetry of the flow, and it accounts for variable gas-phase properties as well as variable liquid-phase viscosities and latent heat of vaporization. In addition, the model considers internal liquid circulation with transient droplet heating, droplet surface regression due to vaporization, and droplet deceleration with respect to the freeflow due to drag.

The slurry droplet calculation was terminated at an early stage when unstable behavior of the velocity and pressure fields over the solid-particle surface caused strong oscillations of the particle accelerations. The sensitivity of the instant of first appearance of the instability on numerical parameters and Reynolds number suggests that the instability is of numerical nature and is a result of the strong dynamic interaction of the liquid and solid phases. Even though our model cannot adequately predict the slurry droplet dynamic and thermal behavior at later stages, it does provide some important insight for the early stable period.

The computed liquid-phase fields for the slurry droplet show that the presence of a large solid particle in the bulk of the liquid-carrier fluid is very important throughout the simulation. Continuous monitoring of the relative position of the solid and liquid constituents of the slurry droplet revealed that the solid particle is inertially lagging the motion of the liquid carrier which is accelerated due to its shear interaction with the gaseous freestream. The axial motion of the particle within the liquid volume was found to be very significant, thus enhancing the internal liquid circulation. The liquid-phase isotherms indicate that convection is the dominant energy transfer mechanism within the slurry droplet. Despite the large spatial gradients of liquid temperature at any specific instant, the temperature within an aluminum particle was found to remain spatially uniform, even though it is temporally varying.

The angular variation of several quantities over the slurry droplet surface showed that the heat and mass transfer coefficients peak at regions close to the front stagnation point of the flow, while the maximum surface temperature occurs at regions closer to the recirculating wake behind the droplet. The results also suggested some condensation of the fuel vapor on the liquid surface near the recirculating wake region.

The effects of solid-particle size and density were also investigated with the slurry droplet model. We found that the displacement of the solid particle from the droplet center is reduced with decreasing particle size and density, when all other conditions remain unchanged. For all slurry droplets considered, a steadily increasing separation of the solid particle from the geometric center of the slurry droplet was found.

The rate of increase of the solid-particle eccentricity during the stable period strongly suggests a high possibility of secondary atomization occurring through penetration of the solid particle through the gas/liquid interface at a subsequent stage. Such an event in a practical system would significantly enhance the liquid vaporization and would expose the solid particle to the hot environment of the combustion gases at a very early stage.

Even though our model provides some interesting trends for the early stages of the combustion of a slurry droplet which contains a large particle in its core, future work is needed to resolve the subsequent unstable stages, and consider other significant effects, such as gas/liquid interface nonsphericity.

Acknowledgments

This work was supported by the Office of Naval Research under Contract N00014-89-J-1135 with Gabriel D. Roy serving as technical monitor. The support of the Pittsburgh Supercomputing Center under an Advanced Computing Resources Grant of the National Science Foundation is greatly appreciated. This research was also supported in part by the University of California, Irvine through an allocation of computer time.

References

[1]Antaki, P. J., "Liquid Vaporization and Combustion from Slurry Fuel Droplets," *Encyclopedia of Environmental Control Technology*, edited by P. N. Cheremisinoff, Vol. 1, Thermal Treatment of Hazardous Wastes, Gulf, Houston, TX, 1989, pp. 179–209.

[2]Law, C. K., Law, H. K., and Lee, C. H., "Combustion Characteristics of Coal/Oil and Coal/Oil/Water Mixtures," *Energy*, Vol. 4, 1979, pp. 329–337.

[3]Wong, S. C., and Turns, S. R., "Ignition of Aluminum Slurry Droplets," *Combustion Science and Technology*, Vol. 52, 1987, pp. 221–242.

[4]Turns, S. R., Wong, S. C., and Ryba, E., "Combustion of Aluminum-Based Slurry Agglomerates," *Combustion Science and Technology*, Vol. 54, 1987, pp. 299–318.

[5]Chung, J. N., "The Motion of Particles Inside a Droplet," *Journal of Heat Transfer*, Vol. 104, Aug. 1982, pp. 438–445.

[6]Petela, R., "Combustion of Mono-Fractional Droplets of Coal/Oil Mixtures," *Fuel*, Vol. 64, 1985, pp. 692–696.

[7]Sitarski, M. A., "Thermal Dynamics of a Small Vaporizing Slurry Droplet in a Hot and Radiant Environment: Feasibility of the Secondary Atomization," *Combustion Science and Technology*, Vol. 71, 1990, pp. 53–75.

[8]Bhatia, R., and Sirignano, W. A., "Vaporization and Combustion of Metal Slurry Droplets," AIAA Paper 91-0282, Reno, NV, Jan. 1991.

[9]Chiang, C. H., Raju, M. S., and Sirignano, W. A., "Numerical Analysis of Convecting, Vaporizing Fuel Droplet with Variable Properties," *International Journal of Heat and Mass Transfer*, Vol. 35, No. 5, 1992, pp. 1307–1324; see also AIAA Paper 89-0834, Reno, NV, Jan. 1989.

[10]Dwyer, H. A., and Sanders, B. R., "Detailed Computation of Unsteady Droplet Dynamics," *Proceedings of the Twentieth Symposium (International) on Combustion*, Combustion Inst., Pittsburgh, PA, 1984, pp. 1743–1749.

[11]Dwyer, H. A., and Sanders, B. R., "Comparative Study of Droplet Heating and Vaporization at High Reynolds and Peclet Numbers," *Dynamics of Flames and Reactive Systems*, Vol. 95, Progress in Astronautics and Aeronautics, AIAA, New York, 1984, pp. 464–483.

[12]Reid, R. C., Prausnitz, J. M., and Poling, B. E., "Vapor Pressures and Enthalpies of Vaporization of Pure Fluids," *The Properties of Gases and Liquids*, 4th ed., McGraw-Hill, New York, 1987, pp. 212–218.

[13]Patankar, S. V., "Convection and Diffusion," *Numerical Heat Transfer and Fluid Flow*, Hemisphere, New York, 1980, pp. 79–111.

[14]Anderson, D. A., Tannehill, J. C., and Pletcer, R. H., "Iterative Methods for Solving Systems of Linear Algebraic Equations," *Computational Fluid Mechanics and Heat Transfer*, Hemisphere, Washington, DC, 1984, pp. 130–138.